STUDY OF $W^{\pm}$ AND Z^{0} IN UA2

The UA2 Collaboration
Bern - CERN - Copenhagen (NBI) - Heidelberg - Orsay (LAL) -
Pavia - Perugia - Pisa - Saclay (CEN)

presented by Kurt Borer
University of Berne, Switzerland

ABSTRACT

A preliminary analysis of high p_T electrons detected in the UA2 experiment at the CERN $\bar{p}p$ Collider ($\sqrt{s}$ = 546 and 630 GeV) has been done. Results on $W^{\pm}$ and Z^{0} production and properties are presented and compared to the expectations from the Standard Electroweak Model. We find good agreement between the UA2 experimental results and theoretical predictions.

1. INTRODUCTION

The UA2 collaboration has already reported experimental results on the processes

$$\bar{p} + p \rightarrow W^{\pm} + \text{anything}^{1)}$$
$$\hookrightarrow e^{\pm} + \nu(\bar{\nu})$$

and

$$\bar{p} + p \rightarrow Z^{0} + \text{anything}^{2)}$$
$$\hookrightarrow e^{+} + e^{-}$$

where $W^{\pm}$ and Z^0 are the Intermediate Vector Bosons (IVB) of the Electroweak Theory. The data were taken at the CERN SPS $\bar{p}p$ Collider in the period 1981-1983 ($\sqrt{s}$ = 546 GeV) and amounted to a total integrated luminosity $\mathcal{L}$ = 142 nb^{-1}. Most of the UA2 results were in agreement with expectations from the Standard SU(3)⊗SU(2)⊗U(1) Model and with the results reported by the UA1 Collaboration on the same subject[4)].

However, the data presented also features that might have suggested the existence of unexpected phenomena. Namely :

i) a $Z^0 \rightarrow e^+e^-\gamma$ was observed in a kinematical configuration having a low probability for internal bremsstrahlung;

ii) 3 events, interpreted as

$$\bar{p} + p \rightarrow W + \text{hard jet(s)},\ W \rightarrow e\nu$$

were found unlikely in terms of a QCD description of the W production mechanism[5)].

These results, together with the observation of unexpected events by UA1[6)], have been at the origin of various theoretical speculations suggesting new physics phenomena beyond the Standard Model.

The subsequent Collider running period, which took place at the end of 1984, was clearly expected to shed more light on these issues.

2. THE 1984 $\bar{p}p$ RUN

In the fall of 1984 the $\bar{p}p$ Collider ran at the higher energy of $\sqrt{s}$ = 630 GeV, as a result of an improved magnet cooling system. Fig. 1 summarizes the performance of the machine during the period. The highest instantaneous luminosity was $\mathcal{L} = 3.5 \cdot 10^{29}$ cm^{-2} s^{-1} and the longest luminosity lifetime was ~ 24 hours[7)]. The total integrated luminosity accumulated by the UA2 experiment was $\mathcal{L}$ = 310 nb^{-1}.

The analyses described here are based on the data from the 1984 run. Cross-sections are calculated separately for the 1984 data and the previous ones, given the different centre of mass energy. For the fit of the mass of the IVB's, the measurement of the W charge asymmetry and the determination of the Z^0 width, the full data sample of the UA2 experiment is used, corresponding to an integrated luminosity $\mathcal{L} = 452\ nb^{-1}$.

All results are preliminary.

3. THE UA2 DETECTOR

The UA2 experimental apparatus has been described in detail elsewhere[8]. Fig. 2 shows a schematic view of its longitudinal cross-section in a plane containing the beam axis. There is complete cylindrical symmetry in azimuth (ϕ), while in polar angle (θ) one can distinguish two regions :

- The central region ($40° < \theta < 140°$) is covered by a highly segmented, tower structured electromagnetic and hadronic calorimeter. The 240 cells of the central calorimeter point to the interaction point.

- The two forward regions ($20° < \theta < 37.5°$ and $142.5° < \theta < 160°$) have been instrumented with the main aim of measuring the forward-backward charge asymmetry of $W^{\pm}$ decays. They are equipped with 24 (12 on each side) identical magnetic spectrometers followed by electromagnetic calorimeters. In front of both the central and the forward calorimeters, preshower counters guarantee an accurate localization of electromagnetic showers to improve the identification of electrons against background.

4. DATA TAKING

Triggers sensitive to high p_T electrons are constructed from calorimeter phototube (PM) signals with gains proportional to transverse energy.

Electromagnetic showers may span across adjacent calorimeter cells. Trigger thresholds were therefore applied to linear sums of signals from 2 x 2 cell matrices. In the central calorimeter, all possible 2 x 2 matrices were constructed; in the forward ones only combinations in a given sector were considered.

There are two triggers sensitive to electrons in UA2 :

- The "W-trigger", for which the signal from at least one matrix must exceed a threshold set at 10 GeV
- the "Z-trigger", for which the signals from at least two matrices, separated by more than 60° in azimuth, must exceed 4.5 GeV.

To suppress background from sources other than $\bar{p}p$ collisions, a coincidence with two signals from hodoscopes at $0.47° < \theta < 2.84°$ on both sides of the collision point was required. These hodoscopes were part of an experiment to measure the $\bar{p}p$ total cross section[9]. Their efficiency to non-diffractive $\bar{p}p$ interactions was estimated to be at least 98%.

Approximately $\sim 1.5 \cdot 10^6$ events were recorded with the W-trigger and $\sim 1.1 \cdot 10^6$ with the Z-trigger in the 1984 run. Both triggers gave a total of $\sim 2 \cdot 10^6$ events corresponding to an integrated luminosity $\mathscr{L} = 310\ \mathrm{nb}^{-1}$.

5. THE ELECTRON ANALYSIS

Figure 3 shows a schematic representation of the signature of various particles or systems of particles in the UA2 apparatus. Shown in the figure is the transverse cross section of a quadrant of the central detector. The forward detectors present similar features with the additional measurement of the track momentum.

There are distinctive characteristics of different particles in each component of the UA2 detector :

a) in the calorimeter, the small transverse and longitudinal extension of the electromagnetic shower distinguishes electrons from particles undergoing nuclear interactions in the calorimeter material (isolated charged hadrons or hadron jets).

b) the presence of a track in the vertex chambers allows to recognize an electron from a photon (or a π^0) which showers electromagnetically in the calorimeter.

c) a particularly dangerous background to electrons is given by the geometrical overlap of an energetic π^0 with a soft charged hadron. The first produces an electromagnetic shower in the calorimeter, while the latter contributes a track and may fake an electron. This background is reduced by the high resolution preshower counter, which allows the precise localisation of the showering particle.

Therefore, the identification of high p_T electrons is based on the following main criteria :

1. the presence of a localised cluster of energy deposition in the first compartment of the calorimeters, with at most a small energy leakage in the hadronic compartment;

2. the presence of a reconstructed charged particle track which points to the energy cluster. The pattern of energy deposition must agree with that expected from an isolated electron incident along the track direction;

3. the presence of a signal in the preshower counter, the amplitude of which must be larger than that of a minimum ionising particle. The geometrical matching of the preshower hit with the projection of the track must be consistent with the space resolution of the counter itself. These features are characteristic of a high energy electron starting a shower in the preshower counter.

In practice, because of the different instrumentation in the central and forward regions, these criteria are applied in different ways in the two detectors.

Details of the electron identification, together with their efficiency to detect electrons, are presented in Table Ia for the central region and Table Ib for the forward ones. An exhaustive description of the cuts is given in previous UA2 publications[10].

It should be noted that most of the applied selection criteria are satisfied only by isolated electrons : the detection of high p_T electrons contained in a jet of high p_T particles is excluded by the present analysis.

Electrons from photon conversions are removed by requiring a hit in at least one of the two innermost chambers of the vertex detector. Furthermore, in the forward detectors the electron candidate is rejected if it is accompanied by another track of opposite sign at an azimuthal separation smaller than 30 mr.

6. THE ELECTRON SAMPLE

In order to reduce the amount of data to be processed in the preliminary W and Z analyses presented at this Conference, a fast filter has been applied to the total event sample.

1. For the W-triggers, it required the presence in the event of an electron-like energy deposition in the calorimeter (i.e. a cluster of cells with small leakage in the hadronic compartment and small radius). The transverse energy deposited in the electromagnetic compartment E_T^{em} was required to exceed 15 GeV. In addition the event was required to have a total energy imbalance in the transverse plane of at least 13 GeV.

2. For the Z-triggers, events were accepted only if at least two electron-like clusters, with azimuthal separation of at least 60°, exceeded $E_T^{em} > 4.5$ GeV, such that their total mass was greater than 30 GeV/c².

Of the total number of $\sim 2 \cdot 10^6$ W and Z triggers, $\sim 1.2 \cdot 10^5$ remain after the filter cuts. These cuts, although very effective in reducing the data sample to be analysed, introduce biases which make the background estimate somewhat uncertain for $p_T^e < 17$ GeV/c or $M_{ee} < 30$ GeV/c². The analysis of the total data sample is in progress, but the results presented here are only concerned with events satisfying $p_T^e > 17$ GeV/c or $M_{ee} > 30$ GeV/c².

After applying the electron cuts we are left with a total of 290 electron candidates with $p_T^e > 17$ GeV/c. The p_T^e distribution is shown in Fig. 4. Candidates with $p_T^e > 25$ GeV/c obtained by the W and Z analyses are indicated in the figure.

7. TOPOLOGY OF THE EVENTS WITH AN ELECTRON CANDIDATE

The sample of 290 electron candidates presented in Fig. 4 contains, in addition to real electrons, fake electrons coming from misidentified high p_T hadrons or jets of hadrons. Depending on whether the electron is real or fake we expect that the event contains either another high p_T lepton (e or ν) or another jet of high p_T hadrons at approximately opposite azimuth.

In order to study the topology of the events with an electron candidate we search for high p_T jets using the jet finding algorithm described in detail elsewhere[11]. We consider the jet activity at opposite azimuth to the electron candidate in a 120° wedge. We define the quantity

$$\rho_{opp} = - \bar{p}_T{}^{e} \cdot \Sigma \bar{p}_T{}^{jet} / |\bar{p}_T{}^{e}|^2$$

where the sum extends to all jets having an azimuthal separation $\Delta\phi > 120°$ to the electron candidate and $p_T > 3$ GeV/c.

We then split the sample of events with an electron candidate in :

a) Events with $\rho_{opp} < 0.2$: this sample contains $W \to e\nu$.
The ρ_{opp} cut is estimated to be (91 ± 3)% efficient, where the error reflects the uncertainty of the Monte Carlo simulation of low energy jets.

b) Events with $\rho_{opp} > 0.2$: this sample includes the $Z^0 \to e^+e^-$ sample. It is dominated by two-jet background with one jet misidentified as an electron and is used to estimate the background contamination to the W-sample.

8. THE $W \to e\nu$ SAMPLE

The total number of W-triggers passing the electron filter cuts is $\sim 1.1 \cdot 10^5$. After applying the electron identification criteria the sample reduces to 257 events, 130 of which satisfy $\rho_{opp} < 0.2$.

The p_T^e distribution of these events is shown in Fig. 5. There are 87 events (71 in the central region and 16 in the forward ones) with $p_T^e > 25$ GeV/c. The background for $p_T^e > 25$ GeV/c is estimated to be 9.0 ± 0.8 events. The p_T^edistribution of Fig. 5 shows a clear Jacobian peak at $p_T^e \sim 40$ GeV/c, a distinctive feature of $W \to e\nu$ decays. Other physics processes also contribute to the electron sample. In addition to the background, shown as a dashed line in the figure, we estimate a contribution of 3.9 ± 0.9 events from $Z^0 \to e^+e^-$ decays in which one electron is not detected and 2.1 ± 0.2 events from $W \to \tau\nu$, $\tau \to e\nu\bar{\nu}$, for the event sample satisfying $p_T^e > 25$ GeV/c.

The solid curve in fig. 5 is the p_T^e distribution expected once all the contributions to the electron sample are taken into account.

8.1 Background to the W electron spectrum

Of the 257 events with an electron candidate, 124 (excluding the $Z^0 \to e^+e^-$ events) have $\rho_{opp} > 0.2$, namely some jet activity at opposite azimuth to the electron candidate itself. Their p_T^e distribution is shown in Fig. 6. The steeply falling spectrum suggests that the sample consists mostly of misidentified jets. Although the presence of real electrons with opposite jets cannot be excluded, we assume that the sample does not contain electrons from W decays. This assumption is valid to the extent that the ρ_{opp} cut does not reject W's produced at high p_T. Should the jet opposite to the electron candidate be lost outside the UA2 acceptance, these events would become W candidates. For this reason we use the sample to estimate the background to W's in the following way. From the $\sim 1.1 \cdot 10^5$ filtered W-triggers we select those events which do not contain energy clusters with $p_T > 17$ GeV/c passing the electron identification criteria described in Table I . We then apply the topology cut in the same way as was done to the electron sample. The distribution of events with $\rho_{opp} > 0.2$, normalized to 124 events, is shown as a solid line in Fig. 6.

The ratio between the two subsamples resulting from the application of the ρ_{opp} cut

$$(\text{jet} + \rho_{opp} < 0.2) \;/\; (\text{jet} + \rho_{opp} > 0.2)$$

gives the probability that in two-jet events one jet is lost outside the UA2 acceptance. This probability decreases from ~ 10% to ~ 2% when p_T increases from 15 to 25 GeV/c.

The background to the 130 W candidates is estimated from the p_T distribution of jet events with $\rho_{opp} < 0.2$ scaled by the factor

$$(\text{"e"} + \rho_{opp} > 0.2) \;/\; (\text{jet} + \rho_{opp} > 0.2)$$

The resulting distribution is shown in fig. 5 as a dashed line.

8.2 Cross section for W production

The cross section for the process $\bar{p} + p \to W^{\pm}$ + anything followed by the decay $W \to e\nu$ is calculated as

$$\sigma_W{}^e = N_W{}^e \;/\; \varepsilon \mathscr{L}\, \eta$$

where $N_W{}^e$ is the observed number of $W \to e\nu$ decays, ε is the overall efficiency of the electron selection criteria, $\mathscr{L}$ is the integrated luminosity and η is the detector acceptance.

We use the 87 events with $p_T{}^e > 25$ GeV/c for which the acceptance is $\eta = 0.65$. The overall efficiency is $\varepsilon = \varepsilon_{\rho opp} \cdot \varepsilon_{cuts} = 0.66 \pm 0.05$. After subtracting contributions from the background, from Z^0 decays with one electron undetected and from the decay ($W \to \tau\nu$, $\tau \to e\nu\bar{\nu}$), we calculate

$$\sigma_W^{e}(630) = 540 \pm 70(\text{stat.}) \pm 90(\text{syst.})\ \text{pb}$$

for the $W^{\pm}$ inclusive production of cross section at $\sqrt{s} = 630$ GeV times branching ratio into $e\nu$. The systematic error accounts for uncertainties on the luminosity $\mathcal{L}$ (15%) and on the cut efficiencies (7%).

An independent analysis based on data from a trigger selecting events with missing transverse energy [12] gives

$$\sigma_W^{e}(630) = 590 \pm 90(\text{stat.})\ \text{pb}$$

in good agreement with the result of the electron analysis.

We have recalculated the cross-section for W production at $\sqrt{s} = 546$ GeV[1b], taking into account a new measurement of the total $\bar{p}p$ cross-section[9] which implies an integrated luminosity of 142 nb^{-1} instead of 131 nb^{-1} as used in Ref. 16.

The result is

$$\sigma_W^{e}(546). = 500 \pm 100\ (\text{stat.}) \pm 80\ (\text{syst.})\ \text{pb}$$

The cross section ratio at the two collider energies is :

$$R = \sigma(630)\ /\ \sigma(546) = 1.08 \pm 0.26$$

where most systematic errors cancel.

All the measured values are in agreement with QCD predictions[13] :

$$\sigma\ (546\ \text{GeV}) = 360\ ^{+110}_{-\ 50}\ \text{pb}$$

$$\sigma\ (630\ \text{GeV}) = 460\ ^{+140}_{-\ 80}\ \text{pb}$$

$$R \qquad = 1.26$$

8.3 The W mass

To extract the value of the W mass we combine the data collected by UA2 in 1984 ($\sqrt{s}$ = 630 GeV) and in previous runs ($\sqrt{s}$ = 546 GeV).

The resulting sample consists of 123 events with an electron having $p_T^e > 25$ GeV/c. The p_T^e distribution is shown in Fig. 7, together with the estimated background (dashed line) and the theoretical distribution of electrons from W decays (solid line).

The mass value is extracted from this sample by comparing the distribution $d^2n/dp_T^e\, d\theta_e$ with that expected from $W \rightarrow e\nu$ decays (θ_e is the measured polar angle).

To calculate $d^2n/dp_T^e\, d\theta_e$ we have used :

- structure functions from Glück et al.[14] to generate the p_L^W distribution
- the p_T^W distribution of Altarelli et al.[15]
- fixed W width at $\Gamma_W = 3.0$ GeV/c².
- the decay angular distribution expected for the standard V-A coupling of W to fermions.

The detector energy resolution is taken into account.

The best fit to the experimental distribution is obtained with

$$M_W = 81.5 \pm 1.0 \text{ (stat.)} \pm 1.5 \text{ (syst.) GeV/c}^2$$

where the systematic error contains a contribution from the overall uncertainty on the energy calibration of the calorimeter (1.5%) and an uncertainty resulting from the p_T^W distribution used to generate the Monte Carlo data. The event wit $p_T^e = 60$ GeV/c has been excluded from the mass fit.

We have also fitted the same two dimensional distribution of a sample obtained with stricter electron cuts, which has much smaller background contamination, and we find the same value for the W mass indicating, as expected, that the fit is not sensitive to the low p_T^e part of the spectrum. The fit is dominated, instead, by the high p_T^e region, which is sensitive to the topology cut ($\rho_{opp} < 0.2$).

To check that the effect of the ρ_{opp} cut is correctly taken into account in our Monte Carlo simulation, we have fitted the transverse mass distribution of the W sample, which has been shown by Monte Carlo simulation to be insensitive to the ρ_{opp} cut. We find the value

$$M_W = 81.2 \pm 0.8 \text{ (stat.)} \pm 1.5 \text{ (syst.) GeV/c}^2$$

in perfect agreement with the one obtained with the fit to the (p_T^e, θ_e) distribution.

8.4 Forward-Backward Charge Asymmetry

The helicity state of the q and $\bar{q}$ forming the W in $\bar{p}p$ interactions is defined by the V-A coupling. As a result the W is procuded with full polarisation in the direction of the $\bar{p}$ beam. Similarly the V-A coupling determines the helicity of the decay products of the W. As a result a distinctive forward-backward asymmetry of the charge lepton must be observed in the decay $W \to e\nu$. In the W rest frame the angular distribution of the charged lepton is expected to be of the form

$$\frac{dn}{d\cos\theta^*} \propto (1-q\cos\theta^*)^2$$

where q is the charge of the lepton and θ^* is the angle between the charged lepton and the direction of the incident proton. The UA2 experiment is equipped with magnetic spectrometers in the angular region $20° < \theta < 37.5°$ and $142.5° < \theta < 160°$, where the sensitivity to the charge asymmetry is expected to be higher.

There are 30 W candidates with $p_T^e > 20$ GeV/c in the forward spectrometers, with an estimated background of ~ 1 event. Their distribution in the (p^{-1}, E^{-1}) plane, where p is the electron momentum with the sign of $(q \cdot \cos\theta^e_{lab})$, is shown in Fig. 8.

The measured asymmetry is

$$\alpha = [(N_p^+ + N_{\bar{p}}^-) - (N_{\bar{p}}^+ + N_p^-)]/N_{tot} = 0.47 \pm 0.16$$

where N_p^+ $(N_{\bar{p}}^-)$ is the number of positrons (electrons) on the proton (antiproton) side, i.e. the right asymmetry, and equivalently for $N_{\bar{p}}^+$ (N_p^-).

The measured value of α is in good agreement with the expected asymmetry

$$\alpha = 0.54 \pm 0.04$$

where the effects of the background, of the $W \to \tau \to e$ decay chain and of the Z^0 events with only one electron detected have been taken into account.

9. THE $Z^0 \to e^+e^-$ SAMPLE

In the 1984 run $\sim 1.1 \cdot 10^6$ Z-triggers have been recorded, of which $\sim 1.5 \cdot 10^4$ passed the filter selection described in section 4.

From this sample we keep only the events which contain at least two energy clusters passing the calorimeter electron cuts described in Table I.

Although the calorimeter cuts applied are not very strict only 111 events remain with a mass of the two electron-like clusters M_{ee} greater than 30 GeV/c^2. The M_{ee} distribution is shown in Fig. 9a and shows that 11 events have a $M_{ee} > 80$ GeV/c^2 with an estimated background of ~ 1 event. After requiring that at least one of the two clusters satisfies all the electron selection criteria the sample reduces to 15 events. Fig. 9b shows their M_{ee} distribution, where one can see that 8 events have $M_{ee} > 80$ GeV/c^2 and no event is in the region $42 < M_{ee} < 80$ GeV/c^2.

Using a sample of two-jet events, we estimate an upper limit of less than 0.15 events as a background under the Z^0 peak.

For a precise assessment of the sample of the 7 events with $M_{ee} < 42$ GeV/c^2 it is necessary to study the spectrum at lower mass values, in order to establish the background level in this region. This study has not been performed yet, because the event distributions in this region are biased by the requirement $M_{ee} > 30\ \mathrm{GeV}/c^2$.

9.1 The Z^0 cross-section

We use the 8 events with $M_{ee} > 80\ \mathrm{GeV}/c^2$ to calculate the Z^0 production cross-section at $\sqrt{s} = 630$ GeV times branching ratio into e^+e^-. Five events have both leptons in the central region, where the efficiency to detect such a pair with the cuts described in the previous section is 86% and the acceptance is 0.34. For the remaining 3 events, in central-forward configuration, the efficiency is 89%, while the acceptance is 0.19.

For an integrated luminosity of 310 nb^{-1} we find

$$\sigma_Z{}^{e}(630) = 56 \pm 20\ (\mathrm{stat.}) \pm 9\ (\mathrm{syst.})\ \mathrm{pb}$$

where the systematic error has been described in section 8.2.

This result is in agreement with a theoretical expectation of 51^{+16}_{-10} pb[13].

As was done for the W, the cross section at $\sqrt{s} = 546$ GeV has been recalculated :

$$\sigma_Z{}^{ee}(546) = 101 \pm 37\ (\mathrm{stat.}) \pm 15\ (\mathrm{syst.})\ \mathrm{pb}.$$

The theoretical calculation from Ref. 13 gives $42^{+13}_{-\ 6}$ pb.

9.2 The Z^0 mass and width

The total UA2 sample of events with two electrons of invariant mass $M_{ee} > 50$ GeV/c^2 is shown in Fig. 10. It amounts to a total of 16 events, 8 at a $\sqrt{s} = 546$ GeV[2] and 8 at $\sqrt{s} = 630$ GeV, corresponding to an integrated luminosity $\mathcal{L} = 452$ nb^{-1}. The masses of the events taken at $\sqrt{s} = 546$ GeV have been very slightly modified with respect to the values published in Ref. 2 after a recalibration of some calorimeter modules in a test beam.

All events have $M_{ee} > 80$ GeV/c^2, where the background is less than 0.2 events.

The Z^0 mass is measured to be

$$M_{Z^0} = 92.4 \pm 1.1(\text{stat.}) \pm 1.4(\text{syst.}) \text{ GeV}/c^2$$

where the systematic error accounts for the 1.5% global energy uncertainty of the calorimeter response. The masses of the individual events are distributed around M_{Z^0} as shown in Fig. 11. The 3 events indicated with an asterisk in the figure are events D, G and H of Ref. 2 which have not been used in the Z^0 mass evaluation for the reasons explained there.

The same event sample has been used to fit a value for the width of the Z^0, Γ_Z. Given the low statistics of the sample available, several statistical estimators of a Breit-Wigner fit to the data have been studied. We quote

$$\Gamma_Z = 2.7^{+2.2}_{-1.6} \text{ GeV}/c^2 \qquad (1)$$

and $$\Gamma_Z < 5.6 \text{ GeV}/c^2 \quad \text{at } 90\% \text{ C.L.}$$

We can obtain an independent estimate of Γ_Z within the standard model from the relation[16]

$$\Gamma_W/\Gamma_Z = (\sigma_W \, \Gamma_{W \to e\nu}/\sigma_Z \, \Gamma_{Z \to ee}) \cdot R$$

where

$$R = \sigma_Z{}^e \ / \ \sigma_W{}^e = 0.137 \ {}^{+0.040}_{-0.034}$$

as a weighted average of the cross sections at the two centre of mass energies. The error on R is statistical only, the systematics cancelling out.

Using the value $\Gamma_W = 2.85$ GeV/c² and the structure function parametrization from Ref. 16, we calculate

$$\Gamma_Z = 2.6 \quad \text{GeV/c}^2 \qquad (2)$$

and $\Gamma_Z < 3.8$ at 90% confidence level, in good agreement with (1).

Within the framework of the standard model, we can compare the measured value of Γ_Z to the expected one to extract the number of additional light neutrinos expected. Taking as expected $\Gamma_Z = 2.82$ GeV/c² and $\Gamma_{Z \to \nu\bar{\nu}} = 180$ MeV/c² we find

$$\Delta N_\nu < 15 \qquad \text{at 90\% C.L.}$$

from (1) and

$$\Delta N_\nu < 5.5 \qquad \text{at 90\% C.L.}$$

from (2).

10. THE $Z^0 \to ee\gamma$ DECAY MODE

As already mentioned in the Introduction, one event of the type $Z^0 \to ee\gamma$ was observed by UA2 in the data taken in 1983. The probability that internal bremsstrahlung can give rise to such, or less probable configuration is 1.4%. Therefore we expected a total of $N_{ee\gamma} = 0.11$ events of this kind in the 1983 Z^0 data sample to come from standard processes.

No such event has been observed in the 1984 data, giving a global expectation of $N_{ee\gamma} = 0.22$ events.

It should be pointed out that configurations where the opening angle between the electron and the photon is less than 20° in θ or 30° in ϕ are not detected by the UA2 apparatus.

11. CONCLUSIONS

Preliminary results on W and Z production and properties have been obtained from the data taken at the SPS Collider at $\sqrt{s}$ = 630 GeV. They confirm previously published UA2 results at $\sqrt{s}$ = 546 GeV. The measurement of the production cross section, the values of M_W, M_Z and Γ_Z, and the measurement of the forward-backward charge asymmetry in W decays all agree with the Standard Electroweak Model and QCD.

From the measured values $M_W = 81.2 \pm 0.8 \pm 1.5$ GeV/c² and $M_Z = 92.4 \pm 1.1 \pm 1.4$ GeV/c² we can extract a value for $\sin^2\theta_W$:

$$\sin^2\theta_W = 1 - M_W{}^2/M_Z{}^2 = 0.228 \pm 0.024.$$

We can also extract $\sin^2\theta_W$ from the relation

$$\sin^2\theta_W = (38.65/M_W)^2 = 0.227 \pm 0.004 \pm 0.009$$

which gives

$$\rho = M_W{}^2/(M_Z\cos\theta_W)^2 = 0.998 \pm 0.03$$

in good agreement with the minimal SU(2)⊗U(1) model.

REFERENCES

1. a) Banner M. et al., Phys. Lett. 122B (1983) 476.
   b) Bagnaia P. et al., Z. Phys. C Part. and Fields 24 (1984) 1.

2. Bagnaia P. et al., Phys. Lett. 129 (1983) 130.

3. For a review see Ellis J. et al., Ann. Rev. Nucl. Part. Science 32 (1982) 443.

4. Arnison G. et al., Phys. Lett. 122B (1983) 103.
   Arnison G. et al., Phys. Lett. 129B (1983) 273.

5. a) Bagnaia P. et al., Phys. Lett. 139B (1984) 105.
   b) For the analysis of highp_T production of W and Z and the measurement of p_T^W and p_T^Z see :
   Plothow-Besch H., Associated production of W's and Z's with jets in UA2, Contribution to this Workshop.

6. Arnison G. et al., Phys. Lett. 139B (1984) 115.

7. Evans L. and Hatton V., CERN-SPS/85-3 (AOP).

8. Mansoulié B., Proc. of the 3rd Moriond Workshop on $\bar{p}p$ Physics (1983) 609.
   See also Ref. 8, 9, 12, 13 of Ref. 1b).

9. Bozzo M. et al., Phys. Lett. 147B (1984) 392.

10. See for example Chapter 4 of Ref. 1b.

11. Bagnaia P. et al., Phys. Lett. 138B (1984) 430.
    See also Pastore F., High p_T Jets in UA2, Contribution to this Workshop.

12. Hänni H., Search for Monojet and Multijet Events with Large Missing p_T in the UA2 Experiment, Proc. of the 5th $p\bar{p}$ Workshop, St. Vincent (Italy) 25 Feb. - 1 March 1985.

13. Altarelli G. et al., CERN-TH 4015/84 (1984).

14. Glück M. et al., Z. Phys. C Part. and Fields 13 (1982) 119.

15. Altarelli G. et al., Nucl. Phys. B246 (1984) 576.

16. Hikasa K., Phys. Rev. D 29 (1984) 1939.

Table I - Electron identification criteria

a) Central detector

Physical quantity	Description	Cuts	Efficiency η (isolated electron)
Calorimeter energy	Radius R_θ, R_ϕ Hadronic leakage $E_{had}/E_{cl} < H_0$	$R_\theta, R_\phi < 0.5$ cells $H_0 = 0.024 + 0.034 \ln E_{cl}$	0.96
Associated track	Track crossing energy cluster. At least one hit in chambers C_1 or C_2.		0.90
Preshower signal	Signal from chamber C_5 within distance d_0 from track intercept.	$d_0 = 10$ mm	0.98
	Associated charge $Q_5 > Q_0$	$Q_0 = 3$ m.i.p.	0.96
	No additional cluster within distance d_1 of selected cluster, with charge larger than Q_5	$d_1 = 60$ mm	0.95
Track-energy cluster match	Require energy pattern to agree with that expected from electron : $P(\chi^2) > P_0$	$P_0 = 10^{-4}$	0.92
		Overall efficiency	0.72 ± 0.05

b) Forward detectors

Physical quantity	Description	Cuts	Efficiency (isolated electrons)
Calorimeter energy	Cluster size $\leqslant$ 2 cells Energy fraction (charged and neutral) in adjacent cells < f_0	$f_0 = 0.05$	1.0
	Energy leakage $E_{leak}/E_{em} < H_0$	$H_0 = 0.02$ *)	0.99
Associated track	Forward track crossing cluster cell. Track minimum distance t from vertex in transverse projection less than t_0	$t_0 = 50$ mm	0.98
	Associated transverse vertex track within $\|\Delta\phi\| < \phi_0$ At least one hit in chambers C_1 or C_2. No identified conversion	$\phi_0 = 30$ mr	0.96
Preshower signal	Signal in each MTPC plane within distance δ_0 of track intercept : $\|\Delta x\| < \delta_x$, $\|\Delta y\| < \delta_y$	$\delta_x = 30$ mm $\delta_y = 20$ mm	0.99
	Associated MTPC charge $Q > Q_0$	$Q_0 \approx 6$ m.i.p.	0.93
Preshower-energy cluster match	Distance of projected MTPC position and cluster centroid as evaluated from PM ratio $\|\Delta x\| < \Delta_0$	$\Delta_0 = 100$ mm	0.98
Momentum	Momentum p and calorimeter energy E satisfy $\|p^{-1}-E^{-1}\|/\sigma(p^{-1}-E^{-1})<\alpha_0$	$\alpha_0 = 2$	0.89 **)
	Overall efficiency		0.75 ± 0.05

*) A cut H = 0.03 is applied if the energy is shared between two adjacent cells.

**) This value takes into account both internal and external bremsstrahlung.

FIGURE CAPTIONS

1. Integrated luminosity per fill as measured by the SPS group during the 1984 Collider period.

2. Longitudinal cross section of the UA2 detector in a plane containing the beam axis.

3. Schematic representation of particle signatures in a quadrant of the UA2 central detector.

4. The electron p_T spectrum of the 1984 data ($\sqrt{s}$ = 630 GeV).

5. Electron p_T distribution of W candidates for the 1984 data sample. The dashed line is the background estimation. The solid line is the fit to the distribution when electrons from all processes are taken into account (see text).

6. P_T distribution of electron candidates (histogram) and of jets (solid line) with $\rho_{opp} > 0.2$.

7. P_T distribution of electrons from $W \to e\nu$ in the entire UA2 data sample ($\mathcal{L}$ = 452 nb^{-1}). The dashed line is the background estimate, while the solid one is the expectation from $W \to e\nu$.

8. Plot of $(p^{-1} \cdot q \cdot \frac{\cos\theta}{|\cos\theta|})$ vs E^{-1} for the 30 $W \to e\nu$ candidate with $p_T^e > 20$ GeV/c detected in the forward regions θ_e is the laboratory angle of the electron with respect to the proton direction.

9. Electron pair mass spectrum of the 1984 data : a) after application of calorimeter cuts on both electron candidates, b) after requiring that at least one of the two candidates be a certified electron.

10. The Z^0 mass peak of the entire UA2 data sample.

11. Mass values and errors of the individual Z^0 candidates. The dashed vertical line corresponds to the fitted M_{Z^0}.

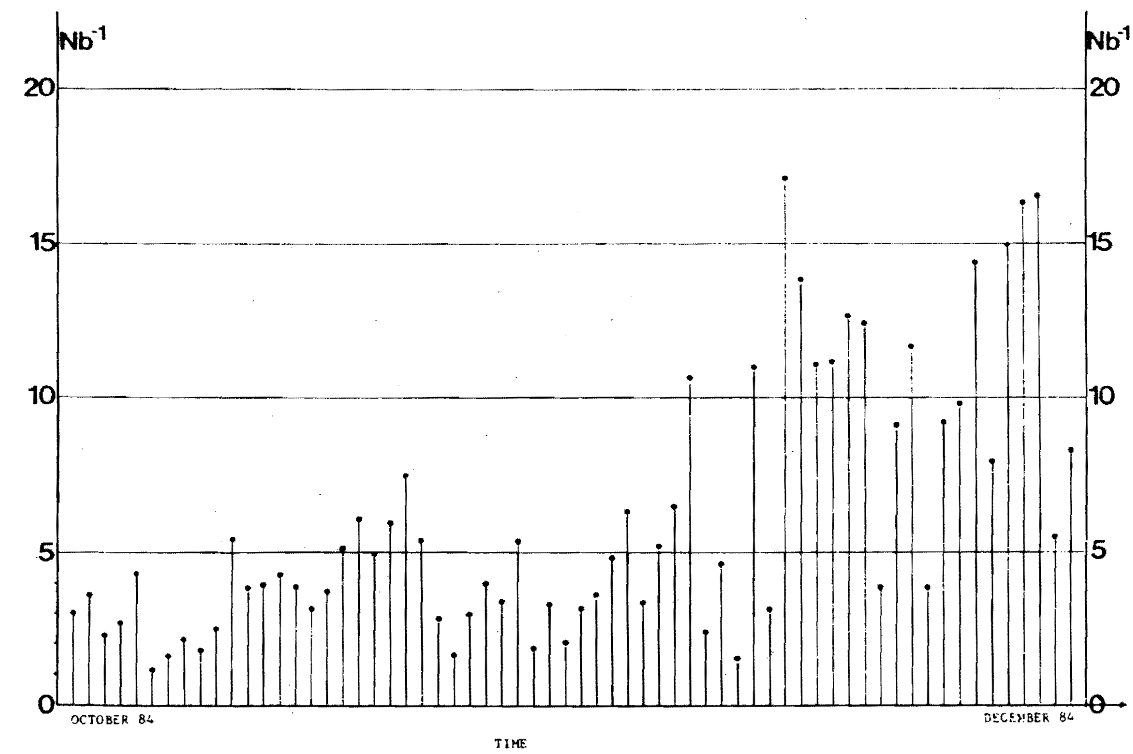

Nb⁻¹
20
15
10
5
0
OCTOBER 84
DECEMBER 84
TIME

Fig. 1

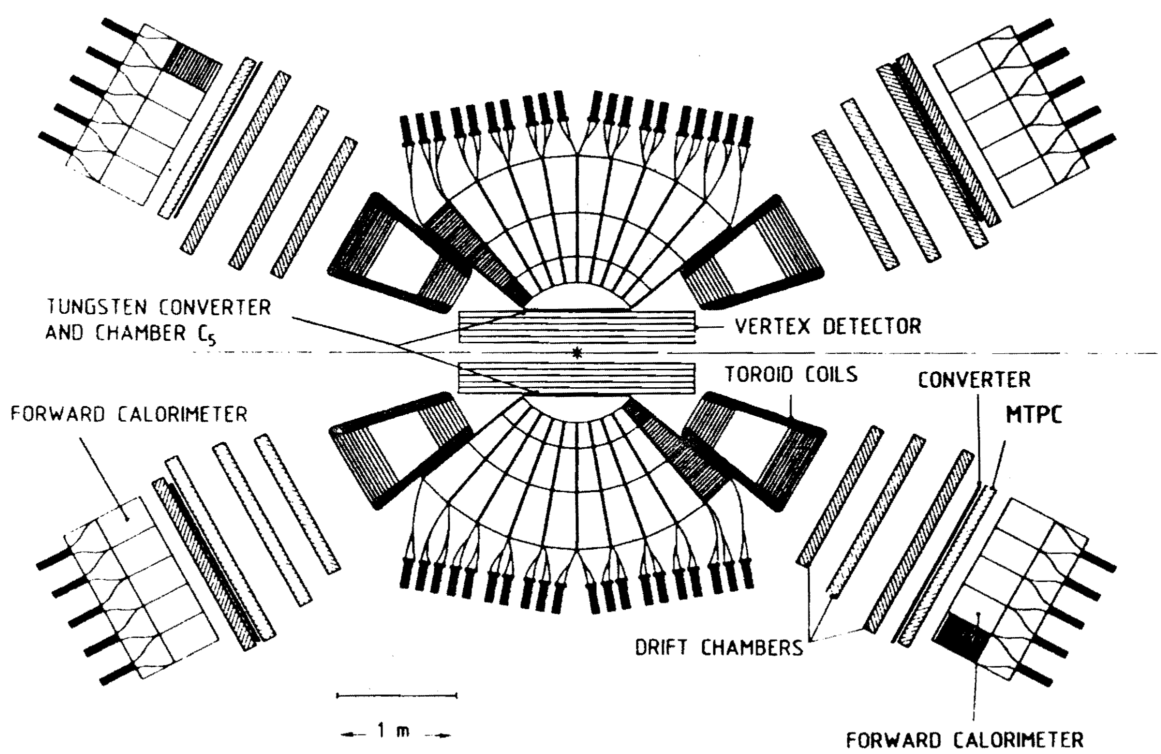

TUNGSTEN CONVERTER
AND CHAMBER C5
VERTEX DETECTOR
TOROID COILS
CONVERTER
MTPC
FORWARD CALORIMETER
DRIFT CHAMBERS
1 m
FORWARD CALORIMETER

Fig. 2

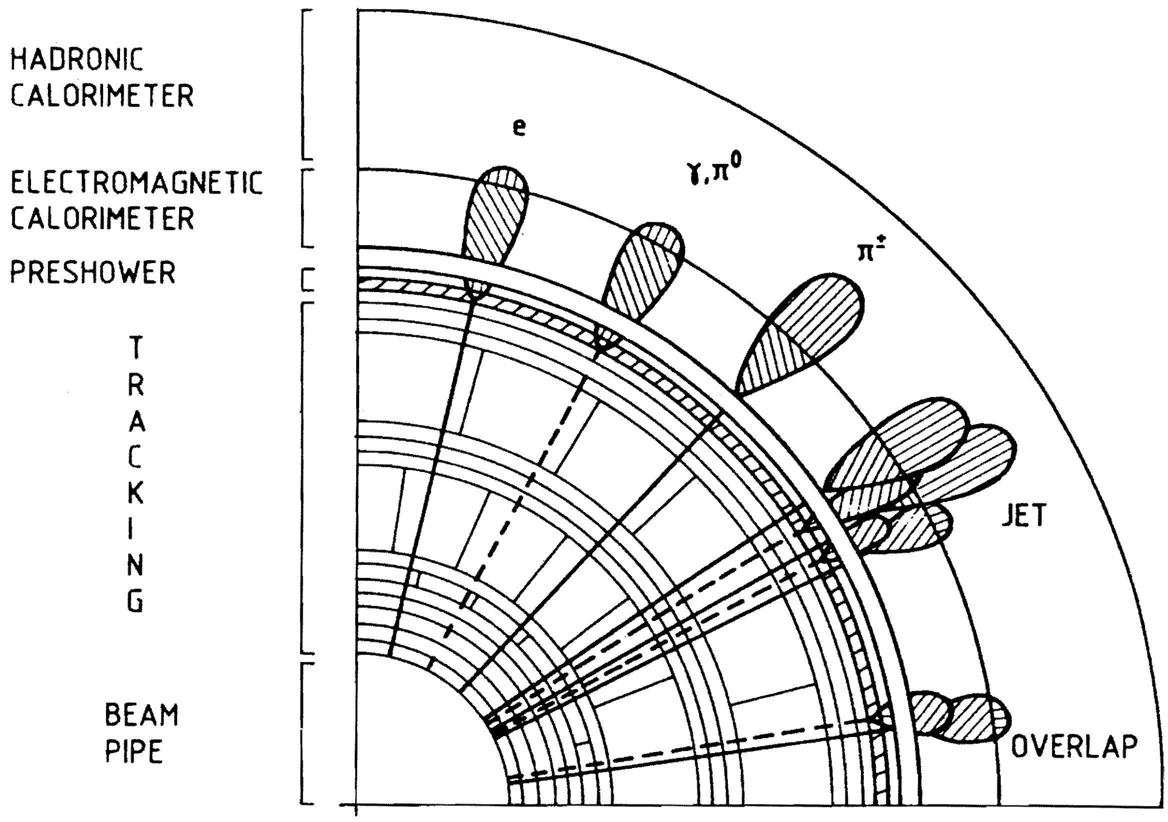
HADRONIC CALORIMETER
ELECTROMAGNETIC CALORIMETER
PRESHOWER
TRACKING
BEAM PIPE
e
γ, π^0
$\pi^\pm$
JET
OVERLAP

Fig. 3

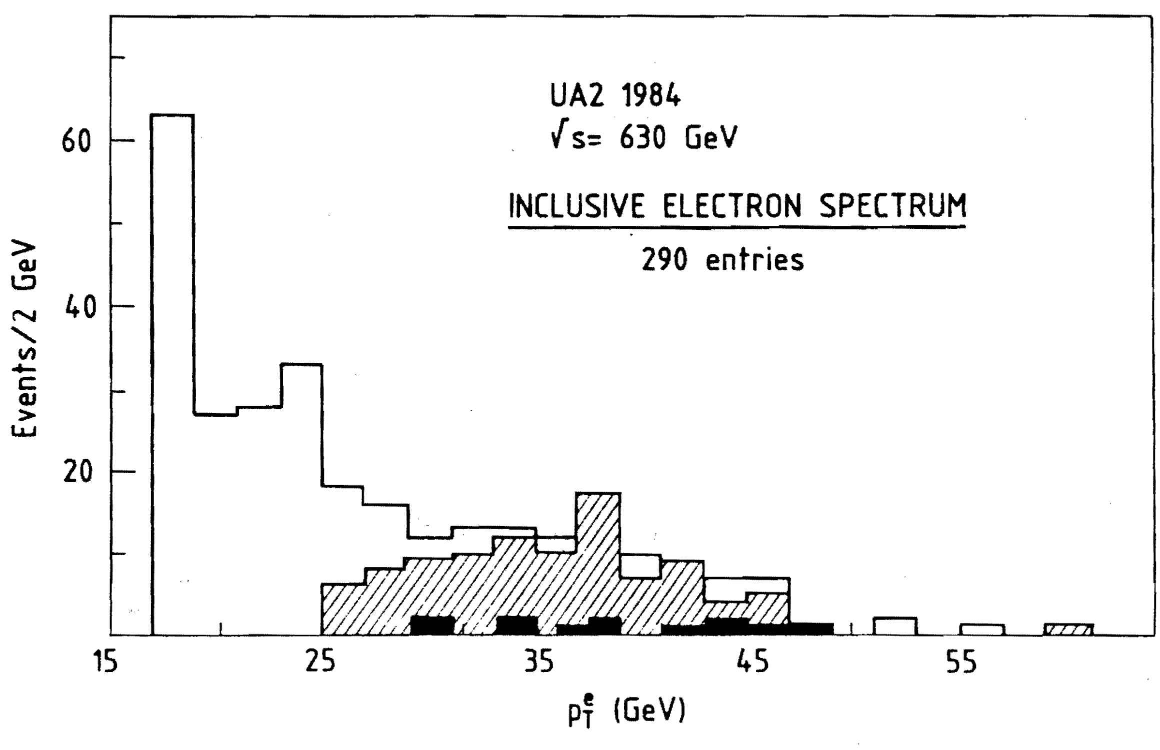
UA2 1984
$\sqrt{s}$= 630 GeV
INCLUSIVE ELECTRON SPECTRUM
290 entries
Events/2 GeV
60
40
20
15
25
35
45
55
p_T^e (GeV)

Fig. 4

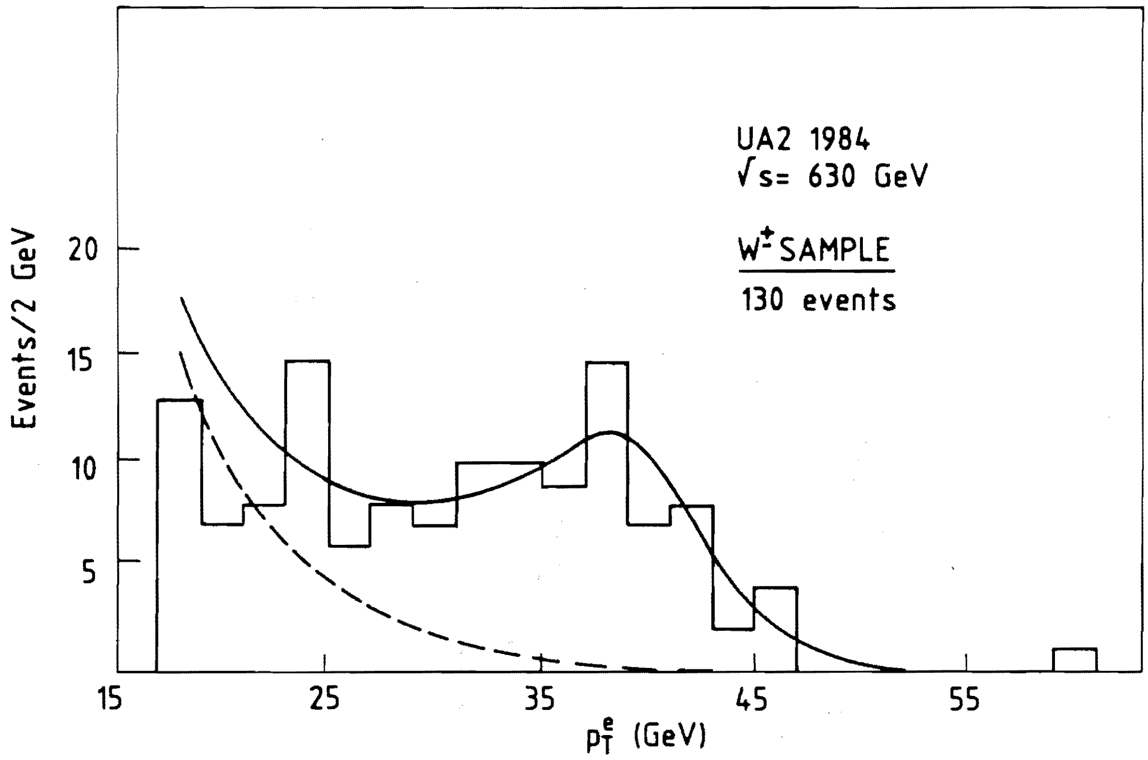
UA2 1984
√s= 630 GeV
W± SAMPLE
130 events
Events/2 GeV
20
15
10
5
15
25
35
45
55
pT^e (GeV)

Fig. 5

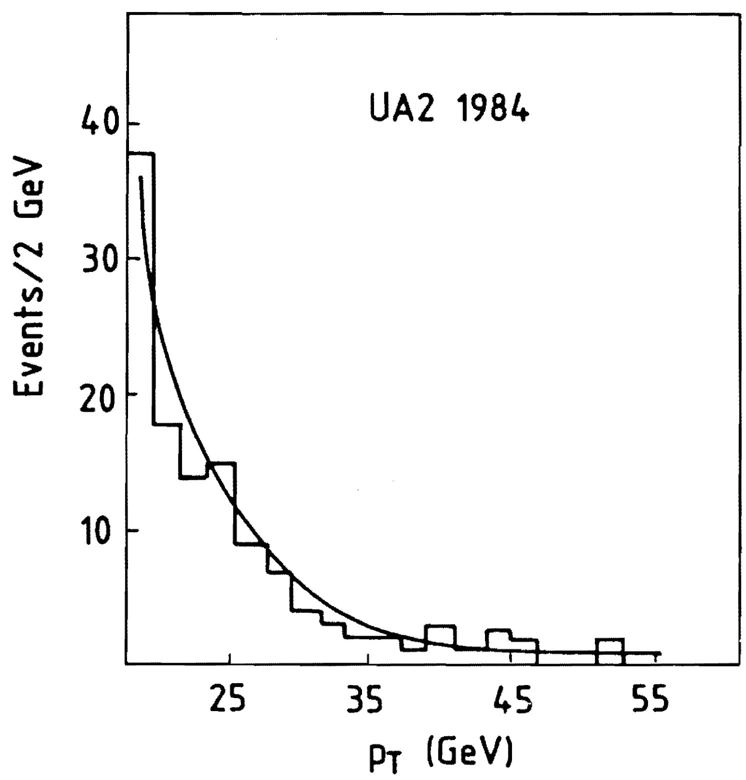
UA2 1984
Events/2 GeV
40
30
20
10
25
35
45
55
pT (GeV)

Fig. 6

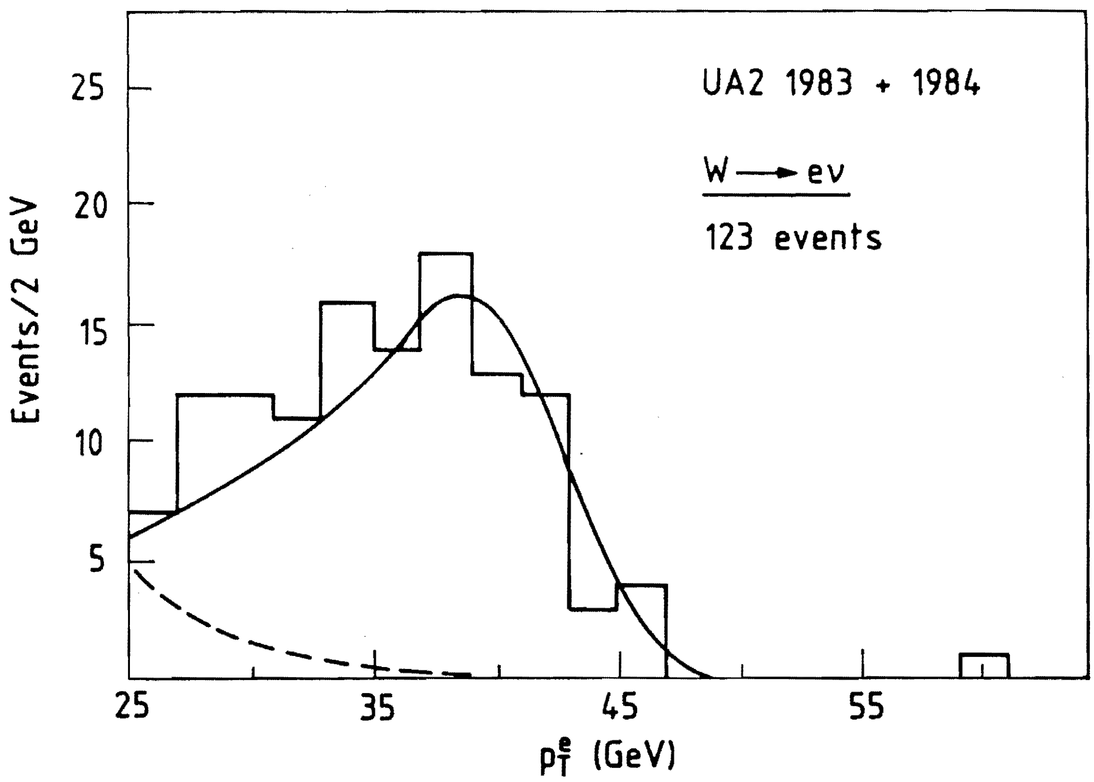
UA2 1983 + 1984
W → eν
123 events
Events/2 GeV
25
20
15
10
5
25
35
45
55
p_T^e (GeV)

Fig. 7

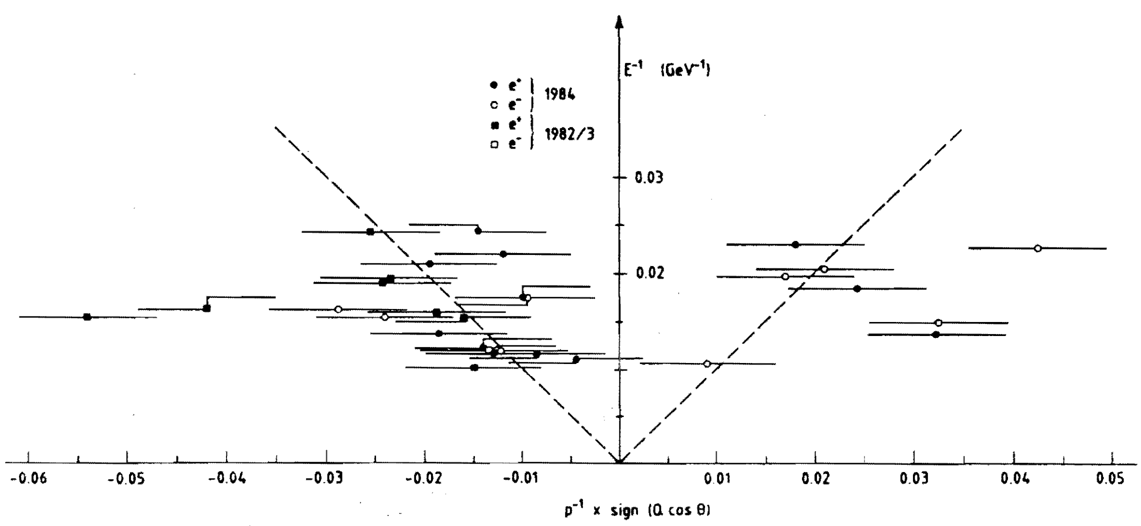
E^{-1} (GeV^{-1})
● e⁺
○ e⁻
1984
■ e⁺
□ e⁻
1982/3
0.03
0.02
-0.06
-0.05
-0.04
-0.03
-0.02
-0.01
0.01
0.02
0.03
0.04
0.05
p^{-1} x sign (Q cos θ)

Fig. 8

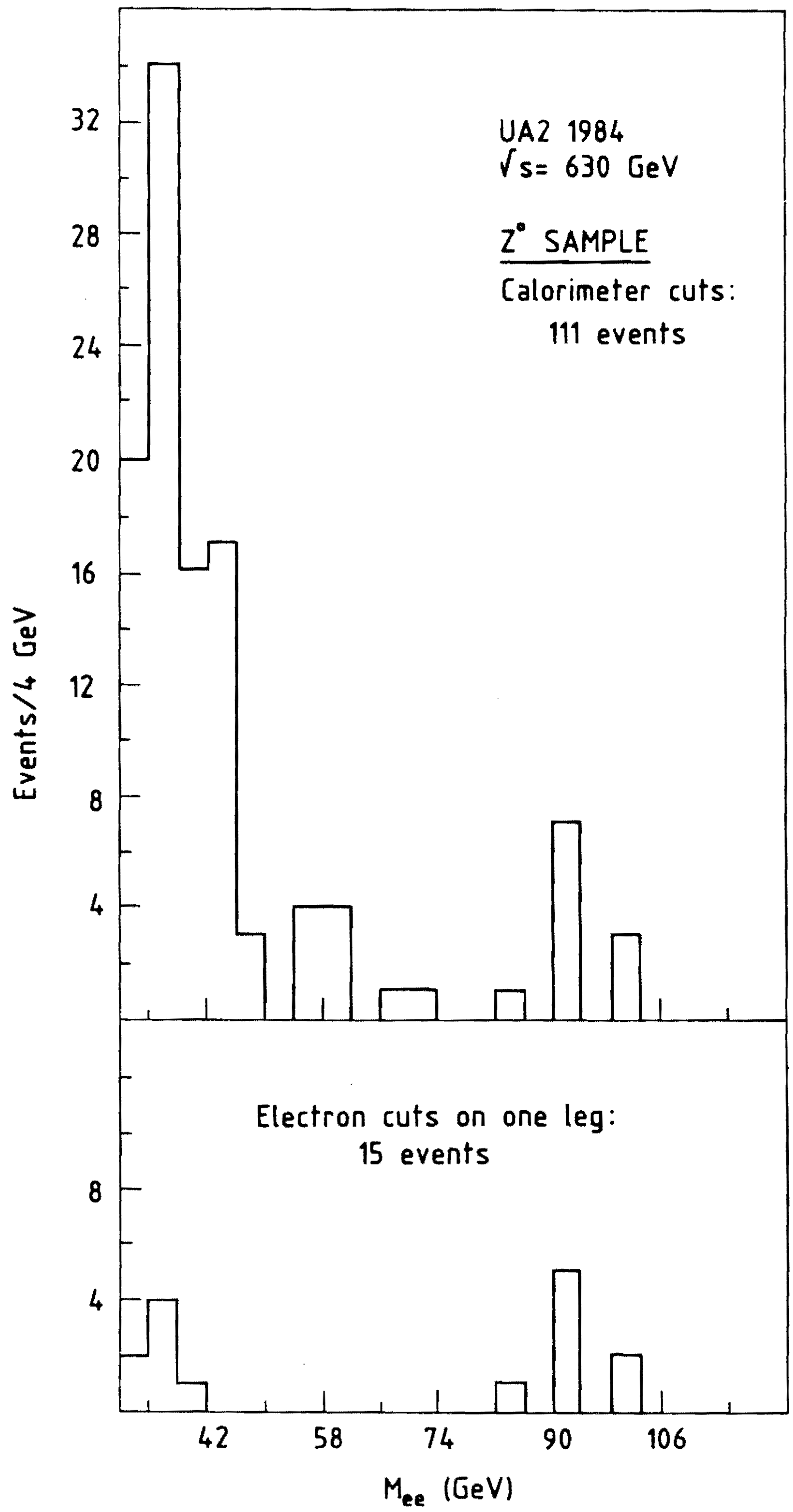
UA2 1984
$\sqrt{s}$= 630 GeV
Z° SAMPLE
Calorimeter cuts:
111 events
Electron cuts on one leg:
15 events
Events/4 GeV
M_{ee} (GeV)
32
28
24
20
16
12
8
4
8
4
42
58
74
90
106

Fig. 9

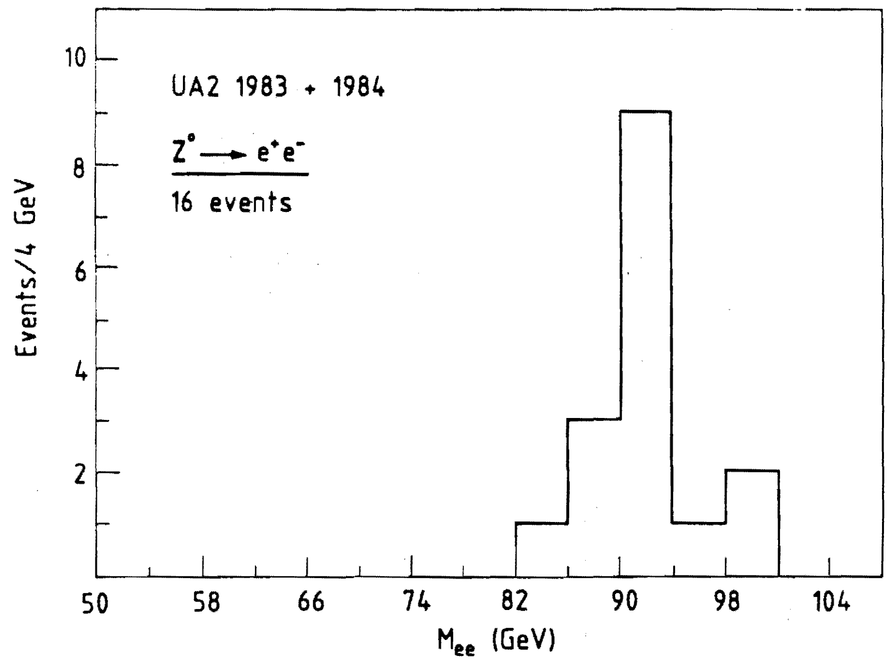
UA2 1983 + 1984
Z° ⟶ e⁺e⁻
16 events
Events/4 GeV
10
8
6
4
2
50
58
66
74
82
90
98
104
M_ee (GeV)

Fig. 10

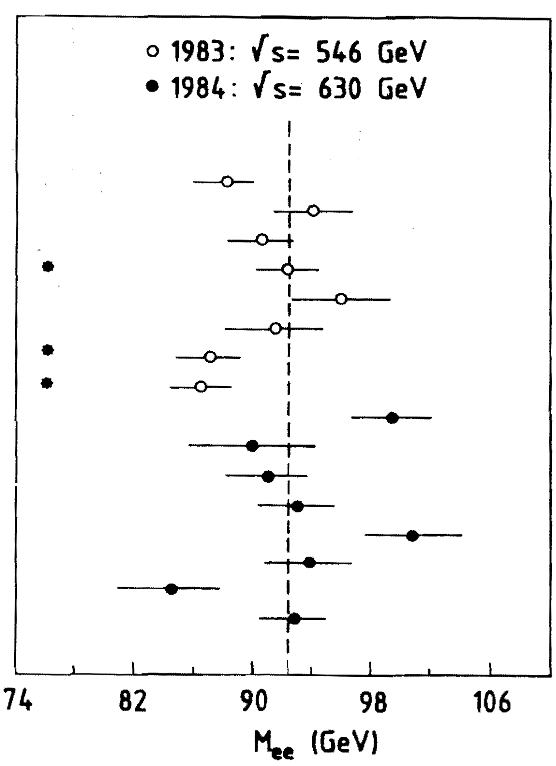
○ 1983: √s= 546 GeV
● 1984: √s= 630 GeV
74
82
90
98
106
M_ee (GeV)

Fig. 11